optica

Distributed optomechanical fiber sensing based on serrodyne analysis

Simon Zaslawski, Zhisheng Yang,* and Luc Thévenaz

Group for Fibre Optics, École polytechnique fédérale de Lausanne (EPFL), Station 11, 1015 Lausanne, Switzerland
**Corresponding author: zhisheng.yang@epfl.ch*

Received 10 November 2020; revised 19 February 2021; accepted 19 February 2021 (Doc. ID 414457); published 12 March 2021

Distributed measurement of forward stimulated Brillouin scattering (FSBS) attracted substantial attention for its ability to probe media surrounding optical fibers. Currently, all techniques extract the information from the FSBS-induced local energy transfer among distinct optical tones, this transfer being fundamentally sensitive to intensity perturbations imposed by nonlinear effects. Instead, here we propose to extract the local FSBS information by measuring the frequency shift of a short optical pulse subject to the phase chirp modulation caused by harmonic FSBS oscillation. In full contrast with existing techniques, the optical pulse is much shorter than the period of the acoustic oscillation, enabling ultrashort spatial resolutions, and its frequency shift is precisely probed by a standard Brillouin optical time-domain analyzer. The proposed technique is validated in both remote and integrally distributed sensing configurations, demonstrating spatial resolutions of 0.8 m and 2 m, respectively, substantially outperforming state-of-the-art techniques.

https://doi.org/10.1364/OPTICA.414457

1. INTRODUCTION

Forward stimulated Brillouin scattering (FSBS) designates the acousto-optic physical process in which two co-propagating light waves couple via the compressive oscillations in their hosting medium of finite cross-section [1–3]. Owing to their tight light confinement as well as long interacting distances and small cross-section, optical fibers are the proper platform to support FSBS and relevant studies have been reported as early as 1985 [2]. FSBS was initially perceived as a stray effect in standard single-mode fibers (SMF) in the form of added phase-noise [2,4], and later reported to offer interesting features for nonlinear amplification in photonic crystal fibers [5]. More recently, FSBS was also proven to induce cross-talk between distinct cores in multicore fibers [6], which can be exploited to realize highly coherent stimulated phonon oscillations [7,8].

Among all possible applications, FSBS has drawn significant attention as a candidate to diversify the quantities probed by fiber sensors, by identifying the substance of a surrounding medium via its acoustic impedance [9]. This method exploits oscillating transverse acoustic waves that convey information from the fiber surroundings to the light confined in the fiber core, requiring no structural modification of standard fibers. This feature is unfortunately hardly exploitable using off-the-shelf SMFs, as the thick protective acrylate coating severely decays the acoustic waves involved in the process [2,10]. The first experimental results were therefore obtained after stripping off the protective coating from a section of optical fiber and immersing it in air, ethanol, and water [9,11]. To mitigate the issue of the fragility of a bare fiber, a thin polyimide coating has been proposed as a promising protective layer due to its excellent acoustic impedance matching with silica and high physical robustness [12,13].

As a step forward, the concept of FSBS sensing integrated over a fiber segment has been extended to distributed (spatially resolved) analysis through the assistance of auxiliary backscattering-based techniques. Using an optical time domain reflectometer (OTDR) [14] or Brillouin optical time domain analyzer (BOTDA) [15], FSBS-induced energy transfer among distinct optical tones can be turned position-resolved, reporting spatial resolutions of 50 m and 15 m, respectively. Alternatively, the local energy transfer can also be interrogated by a broadband Brillouin optical time domain reflectometer (BOTDR) [16] showing a spatial resolution of 8 m. Lately, the spatial resolution has been improved to 2 m by exploiting a dual-pulse BOTDA [17]. Despite the unquestionable progress brought by these pioneering works, they all rely on intensity-based measurement, prone to suffer from a fluctuating power caused by other effects, such as polarization fading [15,16] and four-wave mixing [14,17,18]. In addition, these demonstrations are all realized on a short sensing fiber section (bare or polyimide coated) placed at the far end of a long insensitive fiber (acrylate coated), which can be more qualified for remote short-range distributed sensing than integrally distributed. It turns out to be more challenging to achieve an integrally distributed sensing using existing techniques, as the stronger accumulated energy transfer over the entire fiber length may potentially result in a reduced or even vanishing response, thus giving rise to potential dead zones. So far, the state of the art in integrally distributed FSBS sensing only shows a 100 m spatial resolution over a 1.5 km long polyimide-coated fiber [19], corresponding to 15 resolved sensing points.

In this paper, we propose to exploit the well-known feature that a linearly time-varying phase modulation on an optical wave translates into an optical frequency shift, the so-called serrodyne modulation [20,21]. This is achieved by properly positioning a short optical pulse within the quasi-linear section of the sinusoidal phase modulation caused by locally activated FSBS [15–17,22], and retrieving the local FSBS information by measuring the carrier frequency shift experienced by the pulse. This single-tone frequency-based measurement intrinsically circumvents intensity perturbations undermining existing approaches that are all based on measuring energy transfers among multiple tones. As shown hereafter, we believe this entirely novel approach enables a superior measurement quality in both remote and integrally distributed sensing implementations.

The phase modulation is driven by the temporal response of FSBS under harmonic activation, which is described here by a specific model stating that the optical fiber behaves exactly as a forced damped harmonic oscillator. Once activated by a high-energy intensity-modulated pulse represented by a time-bounded sinusoidal waveform, the free running oscillatory motion field results in a corresponding refractive index modulation on the fiber core, giving rise to a FSBS-dependent net frequency shift over a properly positioned optical pulse. The local FSBS amplitude can be retrieved from the pulse frequency progression that is interrogated by a conventional Brillouin optical time-domain analysis (BOTDA). In addition, the interrogating procedure is designed to make the response intrinsically robust to environmental temperature variations.

The theoretical model, as well as the experimental setup, are first validated in a remote sensing configuration, discriminating between air and ethanol along a 30 m bare fiber appended to a ∼200 m coated SMF with a spatial resolution of 80 cm. This spatial resolution allows a sharp analysis of the fiber geometrical nonuniformity. The setup is then validated to perform a fully distributed sensing over a 500 m long polyimide coated fiber, demonstrating a spatial resolution of 2 m, corresponding to 250 resolved sensing points.

2. PRINCIPLE

The interrogating method presented in this manuscript relies the consideration of an optical fiber as a concatenation of independent cylindrical acoustic resonators. Each of these cavities exhibits a well-defined resonance, which depends not only on the fiber geometrical and mechanical parameters, but also on the acoustic impedance of the material surrounding the fiber [9]. Acoustic waves in such resonators can be activated through electrostriction [23] by launching an intense optical pulse, designated here as the activating pulse, into the optical fiber. Under sinusoidal submodulation (i.e., the activating pulse is modulated in intensity at a frequency f_d, so that many periods of this sinusoidal modulation are contained within the pulse duration, as shown by the orange curves in Fig. 1), each cavity behaves as a forced damped harmonic oscillator (see the detailed derivations in Supplement 1). In driven regime, the oscillating acoustic wave, shown by the purple curves in Fig. 1, builds up and perturbs the local refractive index in the fiber core. When reaching its steady-state, this perturbation $\Delta n(\omega_d, z_0, t)$ at a given fiber location z_0 reads

$$\Delta n(\omega_d, z_0, t) \propto A(\omega_d, z_0)\cos[\omega_d t - \theta(\omega_d, z_0)], \tag{1}$$

where $\omega_d = 2\pi f_d$. $A(\omega_d, z_0)$ is the amplitude response (see dark blue curve in Fig. 1) and $\theta(\omega_d, z_0)$ is the phase lag (see black dashed curve in Fig. 1), which can be respectively expressed as

$$A(\omega_d, z_0) = \frac{A_d(z_0)}{\sqrt{\left[\omega_0^2(z_0) - \omega_d^2\right]^2 + 4\Gamma^2(z_0)\omega_d^2}}, \tag{2}$$

$$\theta(\omega_d, z_0) = \tan^{-1}\left[\frac{2\omega_d\Gamma(z_0)}{\omega_0^2(z_0) - \omega_d^2}\right]. \tag{3}$$

Here, $A_d(z_0)$ is the driving amplitude, which depends on the activating pulse power and the electrostriction coefficient [3], and $\omega_0 = 2\pi f_0(z_0)$, $f_0(z_0)$ is the oscillator natural frequency. The phase θ follows an arctangent function ranging from 0 to π and $\Gamma(z_0)$ is the acoustic damping rate, which strongly depends on the acoustic impedance of the material surrounding the corresponding fiber section [9].

Once the activation is abruptly interrupted, the acoustic field from each cavity oscillator turns free-running at the cavity nominal frequency $f_{\mathrm{fr}}(z_0)$ (see Supplement 1) keeping the phase continuity with the driven acoustic field and decays exponentially, as shown by the light blue curve in Fig. 1. Note that f_{fr} is independent of the driving frequency f_d, and nearly matches the natural oscillating frequency f_0 when damping is moderate. Note also that, although all parameters related to the considered acoustic cavity (A_d, f_0, Γ, and f_{fr}) depend on the current fiber location z_0, this dependency will not be explicitly written hereafter to make equations simpler and clearer.

The refractive index change caused by the freely oscillating acoustic wave is probed through the phase-modulation experienced by a second optical pulse (red pulse in Fig. 1, designated as the reading pulse), which is launched in the fiber with a given time delay Δt with respect to the activating pulse (to avoid detrimental nonlinear interactions between the two optical pulses). The additional phase $\Delta\phi$ experienced by the reading pulse from a single cavity, (i.e., at a given fiber location z_0), reads

$$\Delta\phi(\omega_d, z_0, \Delta t) \propto A(\omega_d, z_0)\cos[\omega_{\mathrm{fr}}(t - \Delta t) - \theta(\omega_d, z_0)]. \tag{4}$$

For a given cavity (A_d, f_0, Γ and f_{fr}), the value of $\Delta\phi$, and consequently the instantaneous frequency $\Delta f = (d\phi/dt)(2\pi)^{-1}$ varies as a function of ω_d and Δt. When setting the reading pulse duration to be shorter than half of the oscillating period $(\pi/\omega_{\mathrm{fr}})$ and setting Δt to let $\omega_{\mathrm{fr}}\Delta t$ be a multiple of 2π, the spectral profile of the net frequency shift experienced by the pulse (i.e. Δf versus f_d), as shown by the green curve in Fig. 1, is similar to the spectral profile of the intrinsic amplitude response A, as shown by the dark blue curve in Fig. 1. This can be intuitively explained by first considering two extreme cases:

1. f_d is far-off resonance (i.e., $f_d \ll f_0$ or $f_d \gg f_0$). In such a situation, θ equals either 0 or π, such that Eq. (4) remains a cosine function, and can be simplified through a limited Taylor's expansion as

$$\Delta\phi(\omega_d, z_0, t) \propto A(\omega_d, z_0)\left(1 - \frac{\omega_{\mathrm{fr}}^2 t^2}{2}\right), \tag{5}$$

where we reasonably kept terms up to the second order assuming a short duration of the reading pulse. The additional instantaneous frequency $\Delta f(f_d, z_0, t)$ experienced by the pulse is therefore given by

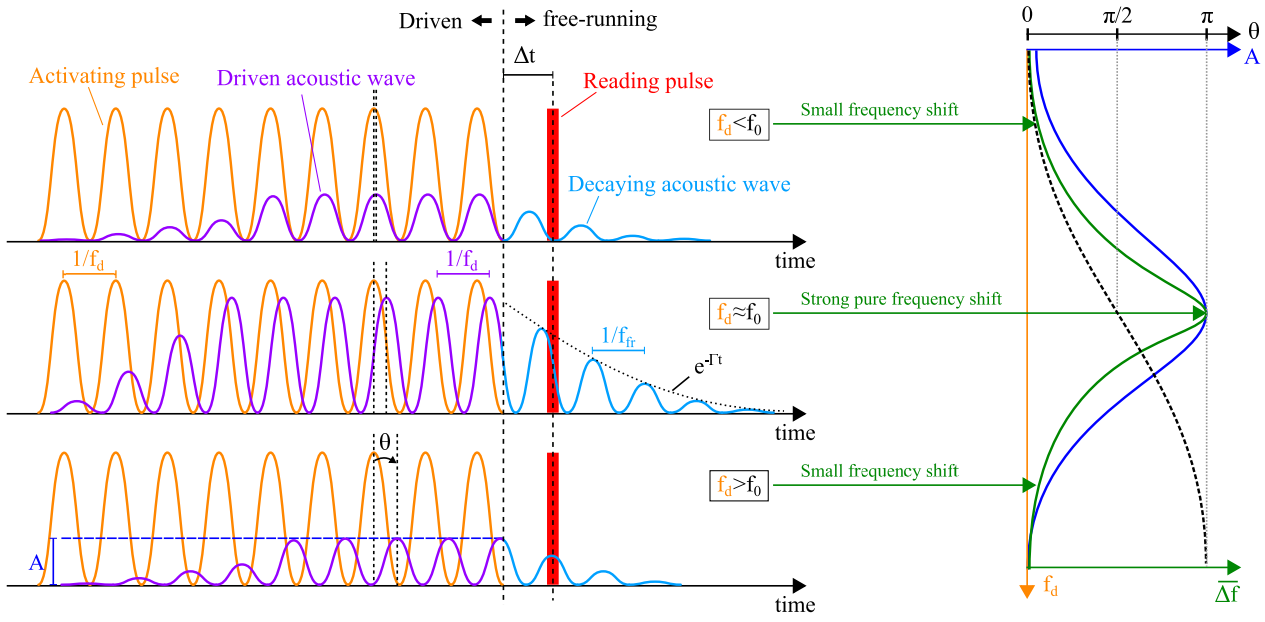

Fig. 1. Acoustic and optical waves temporal profiles at a given fiber location. Due to the additional phase lag θ given in Eq. (3), the phase difference between the acoustic wave and the activating optical pulse is strongly varying as the driving frequency f_d is swept through the FSBS resonance. Refractive index changes resulting from density fluctuations oscillating at a frequency f_{fr} then induce phase modulation on the reading pulse, which translates into a net frequency shift.

$$\Delta f(f_d, z_0, t) = \frac{1}{2\pi}\frac{d\Delta\phi}{dt} \propto A(\omega_d, z_0) 2\pi f_{\mathrm{fr}}^2 t, \quad (6)$$

which describes a linear chirp that broadens the pulse spectrum without changing its carrier frequency. The net frequency shift $\overline{\Delta f(f_d, z_0)}$, which is the average frequency shift over the pulse duration, is zero.

2. f_d is at resonance (i.e., $f_d = f_0$). In such a situation, $\theta = \pi/2$, so that $\Delta\phi$ turns into a sine function. Following the same derivation procedure as in case 1 and keeping only the first-order term in the limited expansion, the phase and additional instantaneous frequency experienced by the short reading pulse can be, respectively, expressed as

$$\Delta\phi(\omega_d, z_0, t) \propto A(\omega_d, z_0)\omega_{\mathrm{fr}} t, \quad (7)$$

$$\Delta f(f_d, z_0, t) = \frac{1}{2\pi}\frac{d\Delta\phi}{dt} \propto A(\omega_d, z_0) f_{\mathrm{fr}}. \quad (8)$$

In this situation, the pulse experiences a pure frequency shift [i.e., $\overline{\Delta f(f_d, z_0)} \propto A(\omega_d, z_0) f_{\mathrm{fr}}$].

Note that both described cases are scaled by the amplitude response of the cavity $A(\omega_d, z_0)$, which is much reduced in the first case and maximum in the second, and by the phase profile overlapping with the short reading pulse, which is quasi-parabolic in the first case and quasi-linear in the second. Based on these considerations, it can be inferred that, as f_d is scanned across f_0, the reading pulse will undergo a net frequency shift $\overline{\Delta f(f_d, z_0)}$, as shown by the green curve in Fig. 1, spanning over a narrower spectral profile than the pure amplitude resonance $A(f_d, z_0)$. As $\overline{\Delta f(f_d, z_0)}$ can be univocally computed from $A(f_d, z_0)$, the acoustic damping rate Γ, which ultimately informs about the material surrounding the fiber [9], can be retrieved by measuring the local net frequency shift $\overline{\Delta f(f_d, z_0)}$ experienced by the short reading pulse. To the best of our knowledge, this is the first technique dedicated to distributed FSBS measurement relying on a frequency-encoded measurement, rather than an intensity-based measurement [14–17] that is intrinsically less robust to intensity perturbations.

3. INTERROGATING PROCEDURE

A standard BOTDA is used to probe the local net frequency shift $\overline{\Delta f(f_d, z_0)}$ experienced by the short reading pulse, which manifests itself as an equivalent shift of the Brillouin gain spectrum generated by this intense reading pulse. Figure 2 schematically presents in detail the interrogating procedure.

Figure 2(a) depicts the pulse sequence launched into the fiber, in which the activating pulse is only present every second reading pulse, the latter playing the role of the pump in the BOTDA. This way, two temporal BOTDA responses at a given probe frequency, with and without FSBS activation, are sequentially obtained in one acquisition window, which is shown in Fig. 2(b). As the temperature and/or strain varies negligibly over such a short time gap (in our case not longer than a few tens of μs, corresponding to a few km), the difference between the two BOTDA responses can be safely considered to be only caused by the FSBS interaction.

By evaluating the peak value of the cross-correlation between the two corresponding Brillouin gain spectra (BGS) at each position along the fiber, as explicated in Fig. 2(c), the accumulated net frequency shift $\overline{\Delta f_{\mathrm{acc}}(f_d, z_0)}$ experienced by the reading pulse up to any position can be obtained. Finally, differentiation on $\overline{\Delta f_{\mathrm{acc}}(f_d, z_0)}$ with respect to distance is carried out to retrieve the local $\overline{\Delta f(f_d, z_0)}$. The setup used to acquire the experimental results shown hereafter are described in Supplement 1.

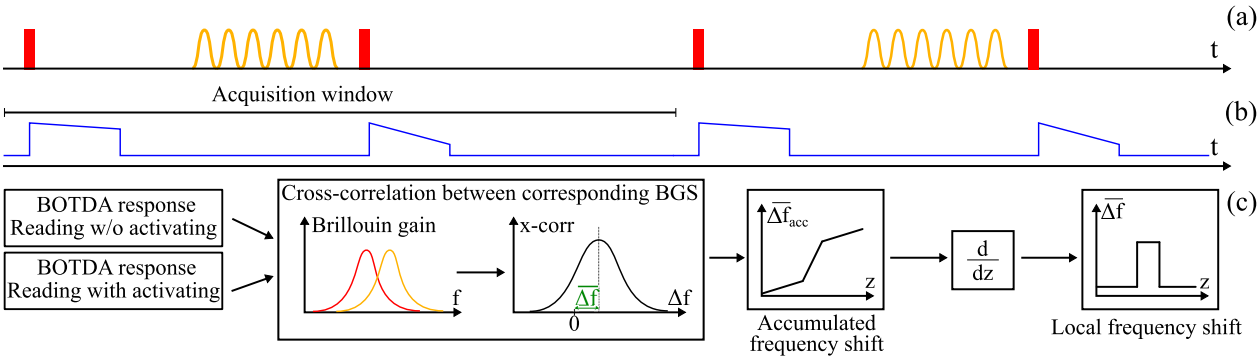

Fig. 2. (a) Pulses sequence launched in the fiber. (b) Brillouin gain at a given probe frequency illustrating the portion of signal acquired. (c) Post-processing yielding the local frequency shift experienced by the reading pulse due to FSBS.

4. RESULTS

A. Remote Distributed Sensing in a Bare Single-Mode Fiber

The validity of the model developed in the theoretical section of this paper is first experimentally demonstrated in a ∼30 m long bare single-mode fiber (SMF), spliced at the far-end of a ∼200 m long standard SMF with acrylate coating. Note that forward stimulated Brillouin scattering (FSBS) is weak in the 200 m SMF as the thick layer of acrylate coating (∼125 μm) severely dampens acoustic waves [2,10], so that only the 30 m bare fiber is suitable for sensing the surrounding material (e.g., air or liquids). This is by far a commonly used approach to evaluate the performance of a distributed FSBS sensor [14–17], though most of the FUT is practically insensitive (i.e., the configuration is indeed referred to as remote distributed sensing). This may prevent some detrimental effects accumulating with FSBS interaction (e.g., nonlocal effect as detailed in Supplement 1), which may turn a critical limiting factor for integrally distributed sensors where all fiber positions are subject to strong FSBS.

For the experiment, a fiber FSBS resonance at ∼130.4 MHz corresponding to the third purely radial mode [9] is selected to be activated (f_d is scanned around 130.4 MHz). In this case the period of the oscillating acoustic wave is ∼8 ns, constraining the maximum duration of the reading pulse to be ∼4 ns [to keep Eqs. (5)–(8) valid] and representing a good trade-off between the FSBS activation efficiency and the BOTDA response. Although the FSBS efficiency is stronger at some higher-order radial modes (e.g., the 7th, at a frequency ∼320 MHz), the substantially shortened reading pulse duration (<1 ns for the 7th radial mode) would significantly lower the BOTDA response [24]; hence, having a significant negative impact on the measurement quality [25]. The power of all optical waves sent into the FUT are carefully adjusted to maximize the signal-to-noise ratio (SNR) and FSBS efficiency, while remaining lower than the threshold of detrimental nonlinear effects, such as backward amplified spontaneous Brillouin scattering for the activating pulse [17] and modulation instability (MI) for the reading pulse [26]. The probe power is set such that the photodetector operates slightly below saturation [27]. All experimental parameters are synoptically presented in Table 1.

After acquiring the Brillouin gain response over the acquisition window shown in Fig. 2(b), the white noise originating from the photodetector is reduced by a numerical Gaussian filter [28] with a bandwidth of ∼125 MHz, leading to an 80 cm spatial resolution

Table 1. Parameters to Remotely Measure FSBS in a Single-Mode Fiber[a]

Activating pulse (width/power)	1 μs/∼3 W
Reading pulse (width/power)	4 ns/∼1 W
Probe power (per sideband)	∼700 mW
f_{RF} (start/interval/# steps)	10.3 GHz/4 MHz/250
f_d (start/interval/# steps)	128.5 MHz/100 kHz/40
Averaging	4096

[a]Optical powers are measured at the FUT input.

that is twice as large as the initial spatial resolution (40 cm determined by the 4 ns reading pulse). This operation, which not only reduces noise but also enlarges the response (as the accumulated frequency shift due to FSBS will be larger over 80 cm than 40 cm), secures a sufficiently high SNR within reasonable measurement time (4096 averages). Figure 3(a) shows the measured 2D map of the Brillouin gain spectrum (BGS), as a function of fiber position and scanning frequency in the absence of activation (see the first half of the acquisition window shown in Fig. 2). The segment of bare fiber is clearly distinguished from the ∼200 m coated segment thanks to their different intrinsic Brillouin frequency shift (BFS, shown by the black curve, obtained by performing quadratic fitting on each local BGS [28]). Figure 3(b) shows the Brillouin gain distribution and the BFS profile when the reading pulse follows the activating pulse (the second half of the acquisition window shown in Fig. 2) with a $f_d = 130.4$ MHz that is close to the FSBS resonance at most fiber positions. Figure 3(c) shows the two-dimensional (2D) map of the cross-correlation of corresponding BGS [column-wise, between Figs. 3(a) and 3(b), following the procedure depicted in Fig. 2(c)]. The spectral position of the maximum of the correlation peak (magenta curve) indicates the trend of the reading pulse frequency shift (accumulated net frequency shift $\overline{\Delta f_{acc}}$) while it propagates along the fiber. A steeper frequency shift (40 MHz over 30 m) can be clearly observed in the bare fiber due to the stronger FSBS interaction.

Based on the accumulated frequency shift $\overline{\Delta f_{acc}}$ obtained in Fig. 3(c), the local net frequency shift $\overline{\Delta f}$ is obtained after numerical differentiation every 80 cm and is shown in Fig. 4(a). Note that we only illustrate $\overline{\Delta f}$ over a section at the fiber far-end for the sake of clarity. The bare fiber is clearly distinguished from the coated region, especially when exposed to air (blue). When immersed in ethanol (red), the signal amplitude drops by a factor ∼5, while remaining well above the noise floor. Note that the large variations of the signal amplitude observed along the bare fiber do

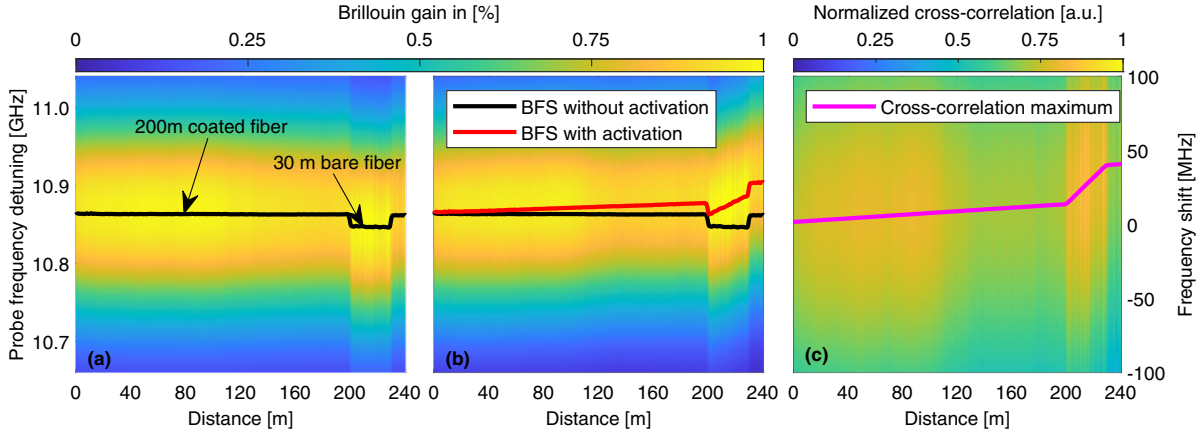

Fig. 3. 2D map of the Brillouin gain response (a) without and (b) with activating pulse. The solid lines show the peak gain frequencies as estimated after data processing. (c) 2D map of the cross-correlation performed column-wise between (a) and (b). The bare fiber is exposed to air and the solid line shows the estimated maximum cross-correlation. For the sake of clarity, the vertical axis of the graphs does not span over the full experimental frequency scanning.

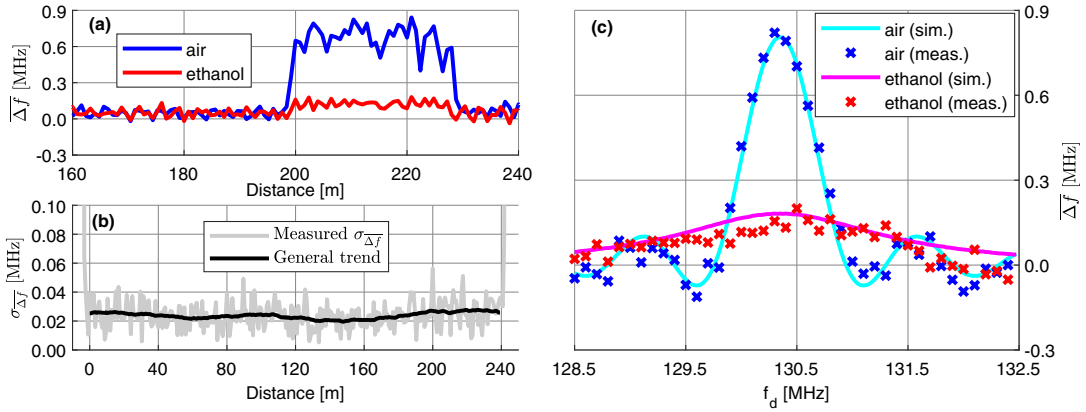

Fig. 4. (a) Frequency shift with respect to distance at a modulation frequency $f_d = 130.4$ MHz when the section of bare fiber is exposed to air (blue) or immersed in ethanol (red). (b) Uncertainty on the measured frequency with a spatial resolution of 80 cm. (c) Retrieved FSBS resonance in the middle of the segment of bare fiber. Solid lines correspond to calculated values from the model.

not result from noise, but originate from a nonuniformity of the FSBS resonance caused by variations of longitudinal strain and/or fiber diameter [10,29], as later discussed in Fig. 5. The negligible impact of noise is corroborated by the experimental uncertainty $\sigma_{\overline{\Delta f}}$ shown in Fig. 4(b), evaluated as the standard deviation among five repeated measurements at a single frequency f_d, which lies below 0.03 MHz over the entire FUT [far smaller than the large variations in Figs. 4(a)]. Figure 4(c) shows the measured (x symbols) and simulated (solid lines) local FSBS spectra in the middle section of the bare fiber. In air, the width of the FSBS response is almost entirely determined by the duration of the activating pulse (1 μs corresponds to 1 MHz). However, the effective acoustic damping rate $\Gamma_e(z)$ $\Gamma_e(z) = \Gamma_m(z) + \Gamma_r(z) + \Gamma_n(z)$ over the local fiber section covered by the reading pulse at position z is the key parameter that must be carefully evaluated to accurately match the simulated profile to the experimental data. It includes the contributions of material damping ($\Gamma_m(z) \sim 2\pi \times 3$ kHz [30]), of reflection loss ($\Gamma_r(z) \sim 2\pi \times 0.5$ kHz [9]), and of geometrical nonuniformity ($\Gamma_n(z)$, resulting from the cladding diameter and strain nonuniformity).

Note that since the local cladding nonuniformity is a priori unknown, estimating $\Gamma_n(z)$ is challenging and it must be specifically calibrated. Taking, for instance, the fiber position shown in Fig. 4(c), $\Gamma_e(z)$ is found to be $2\pi \times 80$ kHz by empirically adjusting $\Gamma_e(z)$ to match the measured spectrum. $\Gamma_n(z)$ is then calculated to be $2\pi \times 76.5$ kHz, showing a dominant contribution to $\Gamma_e(z)$. This value of $\Gamma_n(z)$ lies much lower than the estimated upper bound of $2\pi \times 400$ kHz, directly calculated from the longitudinal fluctuations of the FSBS resonance frequency f_d, shown in Fig. 5 over a 30 m fiber segment, and straightforwardly converted into a 0.3% cladding diameter variation. This suggests that the cladding diameter is fairly uniform over a spatially resolved length (80 cm) at the location shown in Fig. 4(c), regarding the reduced effective resonance broadening due to fiber diameter nonuniformity, broadening that is position-dependent. This also implies that the dominant contribution to damping when the fiber is surrounded by ethanol originates from acoustic loss due to the reduced reflectivity at the glass-liquid interface, which can be theoretically predicted here to be $\Gamma_{(r,eth)} = 2\pi \times 1.1$ MHz [9]. The resulting theoretical curve shown in magenta in Fig. 4(c) using this value shows good agreement with the experimental data (red x symbols).

Figure 5(a) shows the 2D map of the measured FSBS response as a function of f_d and fiber position, the black line depicting the central frequency $f_{fr}(z)$. The fluctuations essentially originate from the fiber geometrical nonuniformity and not from noise,

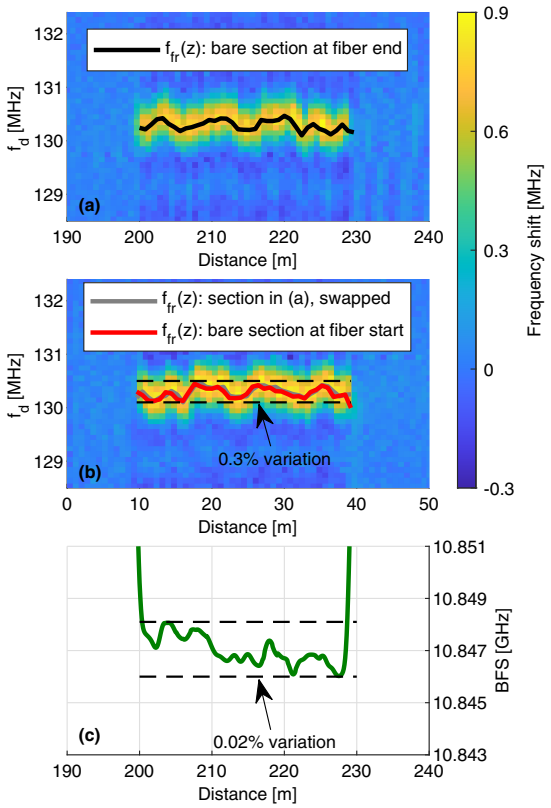

Fig. 5. (a) 2D map of the reconstructed resonance in a section of ∼30 m of bare fiber located after ∼200 m of coated fiber. (b) Same as (a) measured from the other end of the FUT. (c) Brillouin frequency shift (BFS) over the section of bare fiber with activation off.

since a perfect match is obtained by obtaining a mirrored profile after swapping the ends of the FUT [shown in red in Fig. 5(b)] and then superposed on the original profile in the figure (gray).

The 0.3% variation observed in $f_{fr}(z)$ is mostly attributed to the nonuniformity in the fiber cladding diameter. While a nonuniform strain or core doping profile may also induce similar variations in $f_{fr}(z)$, this contribution can be largely ruled out as it is not equally reflected in the ∼0.02% relative BFS changes observed in Fig. 5(c) [31].

It is worth mentioning that, in addition, this technique also enables the resolution of changes in the fiber cladding diameter with such a sharp spatial resolution (80 cm). It can therefore potentially be used to assess imperfections in the physical dimensions of optical fibers or even waveguides, provided that the spatial resolution can be sufficiently reduced.

It must be pointed out that such a large variation in $f_{fr}(z)$ highlights the need for the dedicated calibration mentioned in Fig. 4, since different fiber positions may be subject to significantly different FSBS resonances depending on the underlying, local nonuniformities of the cladding diameter. The results also indicate that coarser spatial resolutions will inevitably result in broader observed FSBS resonances, as confirmed by results in previous reports [14–17].

B. Integrally Distributed Sensing in a Polyimide-Coated Fiber

In this section, we demonstrate the applicability of our method to integrally distributed sensing in a 500 m SMF coated with a thin layer (10 μm) of polyimide. Polyimide has proved promising in FSBS sensing due to its better acoustic impedance matching compared to standard acrylate while preserving the fiber mechanical strength [13,19]. Although weaker than in bare fibers, FSBS activation in polyimide coated fibers remains significantly larger than in conventional acrylate-coated SMFs.

Table 2. Parameters Used to Measure FSBS in a Polyimide-Coated Single-Mode Fiber[a]

Activating pulse (width/power)	1 μs/∼1 W
Reading pulse (width/power)	4 ns/∼1 W
Probe power (per sideband)	∼700 mW
f_{RF} (start/interval/# steps)	10.3 GHz/8 MHz/180
f_d (start/interval/# steps)	123.5 MHz/100 kHz/50
Averaging	4096

[a]Optical powers are measured at the FUT input.

Note that a recent study by *Diamandi et al.* [19] shows that the mechanical behavior of this structure (i.e., a clad cylindrical rod), is far more complex than a bare fiber, especially when immersed into a fluid (e.g., ethanol). The resonance frequency and the decay rate of some acoustic modes turn out to be extremely sensitive to any variations in either the cladding or coating diameter, even when such nonuniformities lie below standard manufacturing tolerances (1%). As will be shown by our results, this may complicate the accurate identification of the fluid surrounding the fiber, since the evaluated equivalent damping rate also turns highly sensitive to the fiber local geometrical parameters.

In this experiment, the activating pulse power is dropped by a factor ∼3 with respect to the previous configuration to avoid detrimental nonlocal effects arising from the phase-shift accumulated over 500 m of FUT (see Supplement 1). This reduction in the FSBS activation limits the experimental spatial resolution to 2 m, which remain acceptable and, to the best of our knowledge, the highest spatial resolution achieved for an integrally distributed FSBS sensor (i.e., in which the impact of FSBS on the signal is of similar importance all over the fiber length). The experimental parameters are synoptically presented in Table 2.

Figure 6(a) shows the 2D mapping of the cross-correlation spectra and the accumulated frequency shift experienced by the reading pulse [similar to Fig. 3(c)] when the activating frequency $f_d = 126$ MHz lies within a FSBS resonance of the fiber, corresponding here to the third purely radial mode (the fiber cladding diameter is 80 μm). Compared to Fig. 3(c), which shows a sharp frequency shift of ∼40 MHz over the ∼30 m bare fiber, the carrier frequency of the reading pulse undergoes this time a shift of ∼160 MHz over the entire fiber length of 500 m.

Figure 6(b) shows the 2D map of the reconstructed FSBS resonance, while the black curve represents the corresponding peak resonance frequency $f_{fr}(z)$, with a variation of ∼0.7% attributed to irregularities in the cladding and/or coating diameter. The FUT ends are then swapped and the mirrored measurement confirms that the frequency profile $f_{fr}(z)$ is the actual intrinsic response of the fiber. Figure 6(c) corroborates this statement, showing good agreement between the initial frequency profile when mirrored (gray line) and the newly frequency profile measured after swapping the ends of the FUT (red line). This good match also indicates a negligible impact of any other nonlinear effect that could further shift the frequency of the pulse during its propagation along the fiber, such as self-phase modulation.

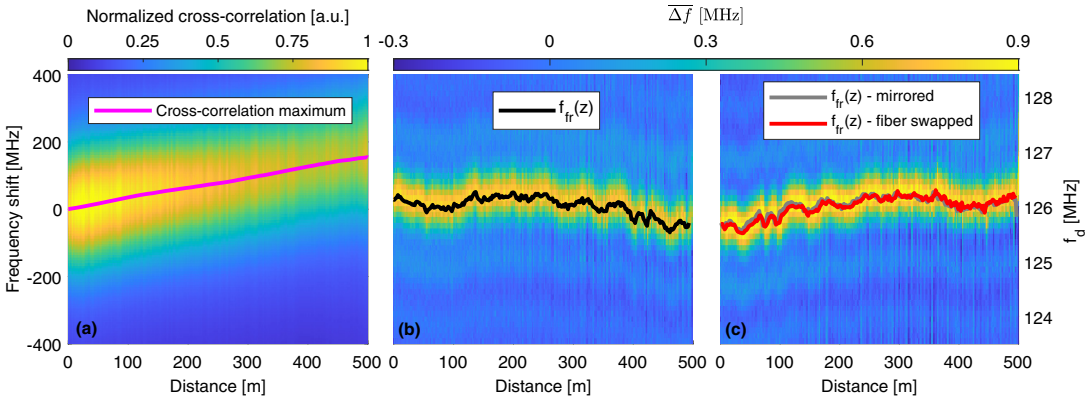

Fig. 6. 2D maps of (a) the cross-correlation between the Brillouin gain spectra of the fiber with activating pulse on and off, (b) the retrieved FSBS resonance along the 500 m polyimide fiber, and (c) the retrieved FSBS resonance obtained with swapped fiber ends.

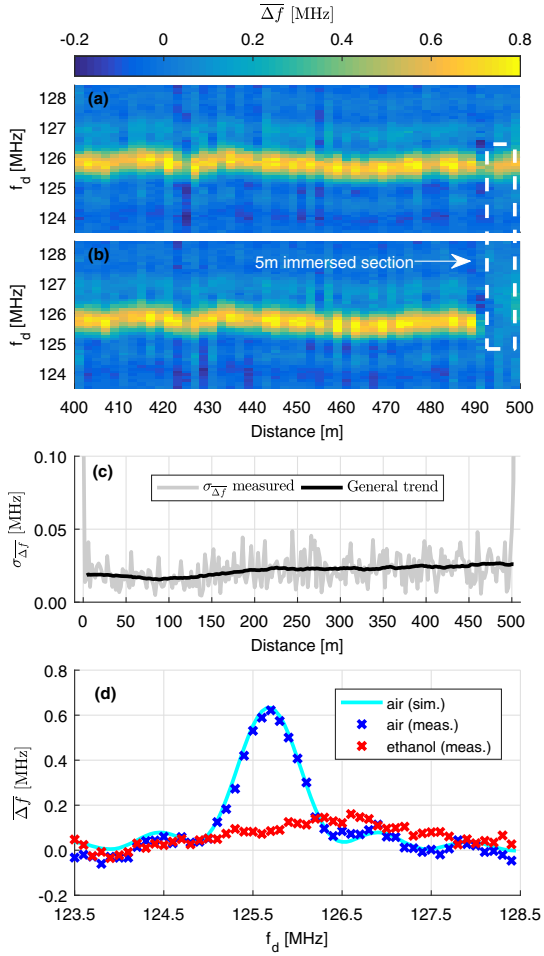

Fig. 7. 2D map of the retrieved FSBS resonance over the last 50 m of sensing fiber when the last ∼5 m are exposed to (a) air and (b) ethanol. (c) Uncertainty on the measured frequency with a spatial resolution of 2 m. (d) Retrieved FSBS within the 5 m probing section.

The sensing capability of our method is illustrated in Fig. 7, where the fiber is used to discriminate between the air and ethanol. Figure 7(a) depicts the 2D map of the FSBS resonance over the last 50 m of sensing fiber when the entire FUT is exposed to air, while Fig. 7(b) shows the same map while a ∼5 m fiber section at the far end of the FUT is immersed into ethanol, showing a significantly lower response that is perfectly discerned from the neighboring points where the fiber lies in air.

The experimental uncertainty $\sigma_{\overline{\Delta f}}$ achieved with 2 m spatial resolution remains below 0.04 MHz over the entire fiber, which indicates a good measurement quality, given that the value is much smaller than the frequency shift at resonance (0.6 MHz in air and 0.15 MHz in ethanol), as demonstrated in Fig. 7(c). The uniform distribution of the frequency uncertainty along the fiber shown in Fig. 7(c) also indicates the negligible impact of any possible nonlinear effect. The FSBS resonances measured in air (blue) and ethanol (red) are shown in Fig. 7(d). The spectrum in air is once again compared to our theoretical prediction with an equivalent damping rate of $\Gamma_{(e,air)} = 2\pi \times 240$ kHz, the fitted curve showing an overall good agreement with the measurement. The resonance measured in ethanol results from a complicated mix of several individual spectra, each exhibiting different central frequencies and damping rates as a result of the enhanced response bias brought by the presence of several layers of varying thickness [19], challenging the accurate evaluation of a unique damping rate reflecting the exact nature of the fluid surrounding the fiber.

5. CONCLUSION

Our technique brings conceptual novelties by (1) overcoming the hard limit of existing techniques that the reading pulse must cover several periods of acoustic oscillations, opening the avenue to submetric spatial resolutions; and (2) designing a single-tone interrogation scheme inherently immune to nonlinear limitations existing in multitone reading processes. This has enabled us to perform (1) remote distributed sensing over 30 m of bare fiber at the far end of a ∼200 m acrylate-coated fiber, demonstrating a spatial resolution of 80 cm after 4096 averages; and (2) integrally distributed FSBS sensing, demonstrating a 2 m spatial resolution over a 500 m long polyimide-coated fiber. This corresponds to 250 resolved sensing points, representing a significant progress toward applicable distributed FSBS sensing when compared to the only reported values (100 m of spatial resolution over 1.5 km, or 15 resolved sensing points) [19]. While this significant improvement is a direct consequence of the core idea of a single-tone reading mechanism, which we firmly believe is a preferred avenue to suffer less from intensity fluctuations induced by perturbing effects, here are a few main perspectives and limitations of our technique:

1. The unmatched sharp resolution enables the evaluation, on a local scale, of nonuniformities in the cladding diameter of the sensing fiber, which are directly reflected by the measured variations in the central frequency of the FSBS resonance. This makes it a promising tool to identify variations and defects in the geometrical structure of optical waveguides, provided that the spatial resolution can be narrowed down to a meaningful extent.
2. The sensitivity of certain acoustic modes to variations in cladding and/or coating diameter challenges the accurate evaluation of substances surrounding the fiber. While this feature has already been analyzed in great detail [19], the experimental data provided in this manuscript pinpointed the range of influence of such nonuniformities.
3. Deeper studies regarding the practical limitations in terms of the optical power and measuring range imposed by the cumulative impact of FSBS would be of significant interest (e.g., nonlocal effects, as sketched in Supplement 1).
4. While the core effect has been here measured using BOTDA, it can be envisioned that other techniques (e.g., based on reflectometry), might perform similarly or even better, depending on experimental conditions.
5. While solving the power perturbation issue in the FSBS reading process, which is the most striking advantage of our technique over previous reports, the system is still sensitive to power fluctuations experienced by the activating pulse (e.g., an abrupt loss point in the fiber due to an external interference). This is a common issue shared by all techniques relying on the pre-activation of acoustic waves.
6. The access to the local FSBS response still requires a numerical differentiation operation, which inevitably enhances the noise. This feature is, however, inherent to the forward scattering nature of FSBS. Although it is highly desirable to bypass this operation, it is not clear at this stage, to the best of our knowledge, whether or not this is achievable. Therefore, it could be an interesting topic to be studied in the near future.

Funding. Swiss National Science Foundation (178895).

Disclosures. The authors declare no conflicts of interest.

Supplemental document. See Supplement 1 for supporting content.

REFERENCES

1. E. K. Sittig and G. A. Coquin, "Visualization of plane-strain vibration modes of a long cylinder capable of producing sound radiation," J. Acoust. Soc. Am. **48**, 1150–1159 (1970).
2. R. M. Shelby, M. D. Levenson, and P. W. Bayer, "Guided acoustic-wave Brillouin scattering," Phys. Rev. B **31**, 5244–5252 (1985).
3. A. S. Biryukov, M. E. Sukharev, and E. M. Dianov, "Excitation of sound waves upon propagation of laser pulses in optical fibres," Quantum Electron. **32**, 765–775 (2002).
4. E. Peral and A. Yariv, "Degradation of modulation and noise characteristics of semiconductor lasers after propagation in optical fiber due to a phase shift induced by stimulated Brillouin scattering," IEEE J. Quantum Electron. **35**, 1185–1195 (1999).
5. P. Dainese, P. St.J. Russell, G. S. Wiederhecker, N. Joly, H. L. Fragnito, V. Laude, and A. Khelif, "Raman-like light scattering from acoustic phonons in photonic crystal fiber," Opt. Express **14**, 4141–4150 (2006).
6. H. H. Diamandi, Y. London, and A. Zadok, "Opto-mechanical inter-core cross-talk in multi-core fibers," Optica **4**, 289–297 (2017).
7. H. H. Diamandi, Y. London, G. Bashan, A. Bergman, and A. Zadok, "Highly-coherent stimulated phonon oscillations in a multi-core optical fiber," Sci. Rep. **8**, 9514 (2018).
8. H. H. Diamandi, Y. London, A. Bergman, G. Bashan, J. Madrigal, D. Barrera, S. Sales, and A. Zadok, "Opto-mechanical interactions in multi-core optical fibers and their applications," IEEE J. Sel. Top. Quantum Electron. **26**, 1–13 (2020).
9. Y. Antman, A. Clain, Y. London, and A. Zadok, "Optomechanical sensing of liquids outside standard fibers using forward stimulated Brillouin scattering," Optica **3**, 510–516 (2016).
10. A. J. Poustie, "Bandwidth and mode intensities of guided acoustic-wave Brillouin scattering in optical fibers," J. Opt. Soc. Am. B **10**, 691–696 (1993).
11. N. Hayashi, Y. Mizuno, K. Nakamura, S. Y. Set, and S. Yamashita, "Experimental study on depolarized GAWBS spectrum for optomechanical sensing of liquids outside standard fibers," Opt. Express **25**, 2239–2244 (2017).
12. H. H. Diamandi, Y. London, G. Bashan, and A. Zadok, "Sensing outside polyimide-coated fibers using guided acoustic waves Brillouin scattering," in *Conference on Lasers and Electro-Optics* (Optical Society of America, 2018), paper SM3K.1.
13. D. M. Chow and L. Thévenaz, "Forward Brillouin scattering acoustic impedance sensor using thin polyimide-coated fiber," Opt. Lett. **43**, 5467–5470 (2018).
14. G. Bashan, H. H. Diamandi, Y. London, E. Preter, and A. Zadok, "Optomechanical time-domain reflectometry," Nat. Commun. **9**, 2991 (2018).
15. D. M. Chow, Z. Yang, M. A. Soto, and L. Thévenaz, "Distributed forward Brillouin sensor based on local light phase recovery," Nat. Commun. **9**, 2990 (2018).
16. S. Zaslawski, Z. Yang, S. Wang, and L. Thévenaz, "Distributed forward stimulated Brillouin scattering measurement using broadband BOTDR," Proc. SPIE **11199**, 323–326 (2019).
17. C. Pang, Z. Hua, D. Zhou, H. Zhang, L. Chen, X. Bao, and Y. Dong, "Opto-mechanical time-domain analysis based on coherent forward stimulated Brillouin scattering probing," Optica **7**, 176–184 (2020).
18. Y. London, H. H. Diamandi, G. Bashan, and A. Zadok, "Invited article: distributed analysis of nonlinear wave mixing in fiber due to forward Brillouin scattering and Kerr effects," APL Photon. **3**, 110804 (2018).
19. H. H. Diamandi, Y. London, G. Bashan, and A. Zadok, "Distributed opto-mechanical analysis of liquids outside standard fibers coated with polyimide," APL Photon. **4**, 016105 (2019).
20. M. Duguay and J. Hansen, "Optical frequency shifting of a mode-locked laser beam," IEEE J. Quantum Electron. **4**, 477–481 (1968).
21. I. Tomita, H. Sanjoh, E. Yamada, and Y. Yoshikuni, "Novel method for generating multiple wavelengths by pulsed serrodyne modulation," IEEE Photon. Technol. Lett. **15**, 1204–1206 (2003).
22. Y. Antman, Y. London, and A. Zadok, "Scanning-free characterization of temperature dependence of forward stimulated Brillouin scattering resonances," Proc. SPIE **9634**, 96345C (2015).
23. R. W. Boyd, *Nonlinear Optics* (Academic, 2008).
24. M. Alem, M. A. Soto, M. Tur, and L. Thévenaz, "Analytical expression and experimental validation of the Brillouin gain spectral broadening at any sensing spatial resolution," Proc. SPIE **10323**, 103239J (2017).
25. M. A. Soto and L. Thévenaz, "Modeling and evaluating the performance of Brillouin distributed optical fiber sensors," Opt. Express **21**, 31347–31366 (2013).
26. M. Alem, M. A. Soto, and L. Thévenaz, "Analytical model and experimental verification of the critical power for modulation instability in optical fibers," Opt. Express **23**, 29514–29532 (2015).
27. S. Wang, Z. Yang, M. A. Soto, and L. Thévenaz, "Study on the signal-to-noise ratio of Brillouin optical-time domain analyzers," Opt. Express **28**, 19864–19876 (2020).
28. S. Zaslawski, Z. Yang, and L. Thévenaz, "On the 2D post-processing of Brillouin optical time-domain analysis," J. Lightwave Technol. **38**, 3723–3736 (2020).
29. G. Bashan, Y. London, H. H. Diamandi, and A. Zadok, "Distributed cladding mode fiber-optic sensor," Optica **7**, 85–92 (2020).
30. B. Auld, *Acoustic Fields and Waves in Solids* (Wiley, 1973).
31. Y. Tanaka and K. Ogusu, "Tensile-strain coefficient of resonance frequency of depolarized guided acoustic-wave Brillouin scattering," IEEE Photon. Technol. Lett. **11**, 865–867 (1999).